VERTEBRATE ZOOLOGY

70 (4): 601 – 613
2020

SENCKENBERG

Morphological and radiographic studies on the skull of the straw-coloured fruit bat *Eidolon helvum* (Chiroptera: Pteropodidae)

Nadja Thier[1,*] & Clara Stefen[1]

[1] Senckenberg Natural History Collections Dresden, Museum of Zoology, Königsbrücker Landstraße 159, 01109 Dresden, Germany — * Corresponding author; nadjathier@gmx.de

Submitted July 7, 2020.
Accepted October 13, 2020.
Published online at www.senckenberg.de/vertebrate-zoology on October 30, 2020.
Published in print Q4/2020.

Editor in charge: Martin Päckert

Abstract

Although 20 % of the extant mammalians are chiropterans, there are only a few studies about their skull morphology. The aim of this work is to broaden the knowledge in this field by investigating *Eidolon helvum* skulls and describing their anatomical characters with a particular focus on general shape, sutures, foramina and processes. We study the external surface of the bones and make a detailed description of 6 rostral bones (nasal, premaxilla, maxilla, palatine, lacrimal, jugal), 9 cranial bones (frontal, parietal, interparietal, pterygoid, sphenoid complex, squamosal, petrosal, ectotympanic, occipital complex) and the mandible. We also make a radiographic analysis by taking X-ray images in lateral and dorsoventral direction. Comparisons with other bats like *Pteropus lylei* and *Desmodus rotundus* show interspecific variations. So this work helps building a solid basis for further phylogenetic, functional or systematic studies.

Key words

Description of individual skull bones, *Eidolon*, morphological, radiographic, subadult individuals.

Introduction

Morphological differences between species are one aspect of phenotypic diversity in mammals and species in general and contribute to biodiversity. As phenotypic diversity is well visible, a long standing question in biology is to understand how phenotypic diversity and associated functional and ecological characteristics evolved. This question is traditionally addressed mainly by comparing morphological characters of fossil and recent species, interpret their function, and compile phylogenies based thereupon. In more recent years, genetic analysis complemented this research and for some phenotypic characters causing genes were found by using mutational screens in the genes of model organisms like *Drosophila* or mouse (e.g., Drysdale, 2001; Gkoutos *et al*., 2004). But the applicability of such approaches to traits across different mammal orders is limited. Moving forward from genetics to genomics, understanding of genetic causes of phenotypic diversity appeared more reachable by genome wide comparisons across many mammalian species. One of these approaches to identify candidate genomic loci that underlie phenotypic differences in mammalian species is "*Forward Genomics*" (Hiller *et al*., 2012, Prudent *et al*., 2016). For successful application this approach has two requirements: a) published whole genome sequences for many species and b) available structured and computer-parsable phenotype data for the species with sequenced genomes. Whereas the first requirement is fulfilled by whole genomes available for > 100 mammal species, the second one turns out to pose a bottleneck, despite of a bulk of zoological literature and numerous zoological collections. But (most of) the information is not available in a structured way across the needed mammals, nor

Table 1. List of examined *Eidolon helvum*-specimens.

Specimen	Sex	Location	Collection date
MTDB14000	male	Lagoa Azul, São Tomé	10.06.1983
MTDB14001	female	Lagoa Azul, São Tomé	11.06.1983
MTDB14002	male	Lagoa Azul, São Tomé	16.06.1983
MTDB14003	female	Lagoa Azul, São Tomé	11.06.1983

Table 2. Skull measurements in mm of *Eidolon helvum*. Skull lengths were measured from the rostral end of the nasals to the caudalmost point of the supraoccipital, skull widths were measured from the maximum points of the parietals, rostrum lengths were measured between the rostral end of the nasals and the front of the orbit and rostrum widths were measured on the level of P4 and M1.

Specimen	**Skull length** [mm]	**Skull width** [mm]	**Rostrum length** [mm]	**Rostrum width** [mm]
MTDB14000	47.85	20.43	16.16	12.10
MTDB14001	46.43	19.09	16.60	12.29
MTDB14002	53.18	20.56	19.09	13.10
MTDB14003	44.61	19.63	15.42	11.39

computer-parsable. Within a project to make *Forward Genomics* work (Hiller *et al*., 2016), a database of morphological traits, numerically coded for 147 mammal species was developed. While compiling this, research gaps concerning the information on phenotypic traits, including basic skeletal morphology of several species of Chiroptera with a completely sequenced genome (see Teeling *et al*., 2018 for compilation) was noted. Thus, with this study we contribute to the filling of the knowledge gap in basic cranial morphology of a bat species. But describing cranial morphology of a (bat) species is more than contributing data ultimately useable for *Forward Genomic* or other concepts in genomic analyses. Morphological studies and descriptions are necessary to understand functions underlying ecological adaptations like feeding behavior, to compile phylogenies, to differentiate species and to fully understand biodiversity not only of bats.

The lack of a standardized reference morphologic description and nomenclature for bats made communication about bat skull morphology difficult and was only recently provided by Giannini *et al*. (2006). This work provides the basis for further phylogenetic, functional or systematic studies particularly as several new species are described constantly (Laureiro *et al*., 2018; Sánchez *et al*., 2019), which are morphologically difficult to differentiate.

Although bats make up one fifth of extant mammalians and are the second largest order after the Rodentia, detailed studies about the morphology of the skull are very rare. In Chiroptera, and particularly in smaller species formerly grouped as microchiroptera the skull bones tend to fuse early so that sutures are not or only hardly visible, which makes them difficult to define. Reyes-Amaya & Jerez (2013) described for the first time the postnatal cranial ontogeny of the common vampire bat, *Desmodus rotundus* (Phyllostomidae), but most studies concentrate on taxonomic (Orihuela, 2011; Hurtado & D'elía, 2018; Lemos *et al*., 2020), morphometric (Juste *et al*., 2001; Budinski *et al*., 2015; Jojić *et al*., 2015) and molecular issues (Giannini & Simmons, 2005; Nesi *et al*., 2013; Demos *et al*., 2019). Some authors even focus on certain regions of the bat skull like Sprague (1943), who investigated the hyoid apparatus, or Wible & Bhatnagar (1996) and Novacek (1985a, b; 1991) who analyzed the ear region and Bhatnagar & Kallen (1974) and Kämper & Schmidt (1977) who studied the ethmoid. For the Yinpteropchiroptera (Springer *et al*., 2001), there is one exceptionally detailed work for *Pteropus lylei* with description about the whole skull, the single skull bones, dentition, foramina and skull development (Giannini *et al*., 2006).

It is the aim of our work to expand the anatomical skull descriptions for Chiropteran species and help filling the gap of knowledge in this field. We choose *Eidolon helvum*, the straw-coloured fruit bat which is one of the most common fruit bats of the African continent. The distribution area ranges from Senegal to Ethiopia to South Africa. The IUCN Red List classed *Eidolon helvum* as near threatened and the population trend is decreasing, as it is threatened by deforestation and by hunting for food and medical use (Cooper-Bohannon *et al*., 2020). *E. helvum* belongs to the family of Pteropodidae which includes 46 genera. The phylogenetic affinity of *E. helvum* has been contentious. Whereas, Bergmans (1997) included *Eidolon* (with two species) in the Rousettini tribe, Almeida *et al*. (2011) support the position as a subfamily by itself.

For the study we had four specimens in our collection and the cranial bones are mostly well demarcated as visible. As pteropodid it is well comparable to *Pteropus* described in detail (Giannini *et al*., 2006). We describe the cranial and rostral skull bones on the external surface and take X-rays of the skull. The anatomical terminology complies with the use in Giannini *et al*. (2006), which is consistent with the Nomina Anatomica Veterinaria (NAV). The study of only few specimens was done with a time constraint within the Project of *Forward Genomics*.

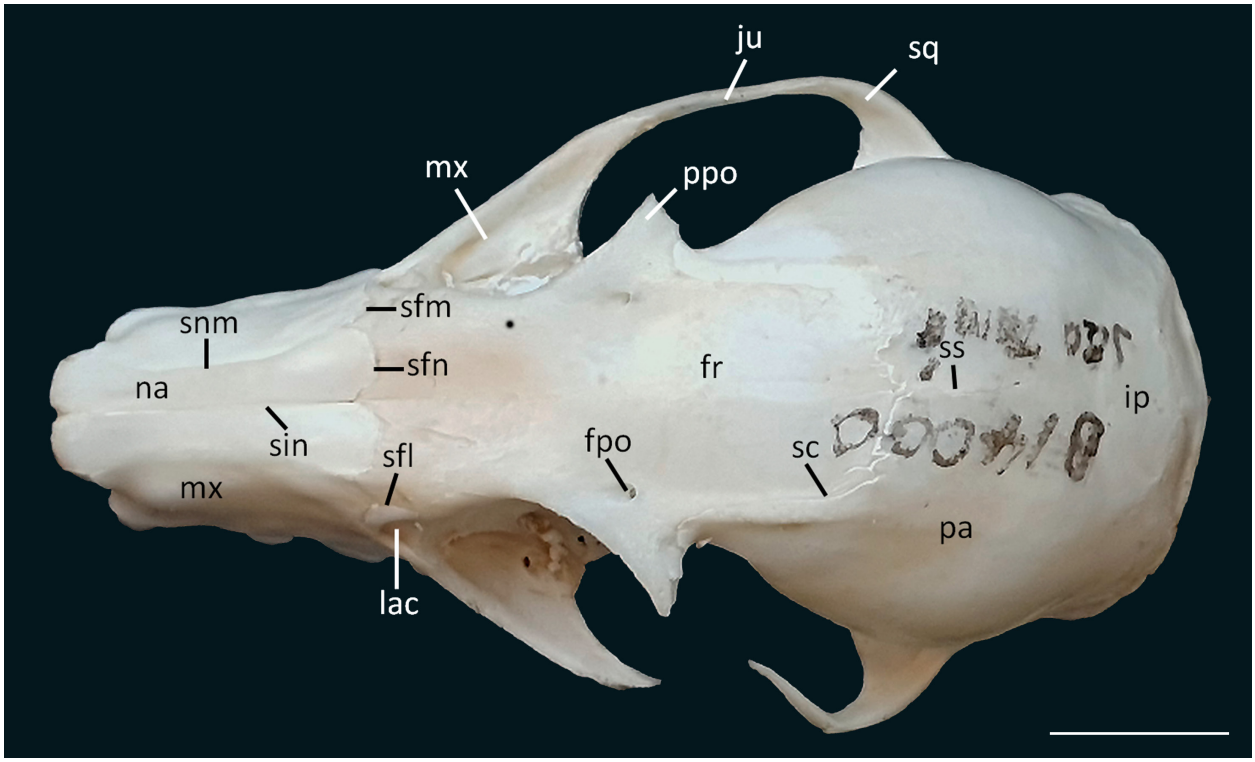

Fig. 1. Dorsal view of the skull of *Eidolon helvum* (MTDB14000). Abbreviations: **fpo** foramen postorbitale, **fr** os frontale, **ip** os interparietale, **ju** os jugale, **lac** os lacrimale, **mx** os maxilare, **na** os nasale, **pa** os parietale, **ppo** processus postorbitalis, **sc** sutura coronalis, **sfl** sutura frontolacrimalis, **sfm** sutura frontomaxillaris, **sfn** sutura frontonasalis**, sin** sutura internasalis, **snm** sutura nasomaxillaris, **sq** pars squamosal ossis temporalis, **ss** sutura sagittalis. Scale bar = 1 cm.

Material and Method

For the present study, four specimens of *Eidolon helvum* skulls of both sexes were available for investigations (Table 1). All specimens are part of the zoological collection of the Senckenberg Natural History Collections Dresden, Museum of Zoology.

The length and width of the cranium and rostrum of all specimens were measured with a digital caliper (150 mm – 0.01 mm; Table 2). Our anatomical descriptions were mainly based on specimen, MTDB14000, a male from São Tomé, an island state in the Gulf of Guinea. We have chosen this specimen, because most of the sutures were visible and thus the bones were unfused. Only visible bones and structures of the external surface were described and no bones were isolated. Comparisons were mostly made with specimen MTDB14002. We examined the specimen MTDB14000 in dorsal (Fig. 1), in lateral (Fig. 2), in ventral (Fig. 3) and occipital views (Fig. 4) as well as the mandible in lateral view (Fig. 5). We also made a radiographic analysis with specimen MTDB14000 and X-rayed the skull in dorsoventral direction (Fig. 6) and lateral (Fig. 7). The X-ray machine we used is a Faxitron LX-60, which calculated the X-ray time automatically.

We follow Giannini & Simmons (2007) in assuming the dental formula for *Eidolon*: I2/2, C1/1, P3/3, M2/3 and use the following nomenclature: the upper dentition represents the incisors I1 and I2, the premolars P1, P3 and P4, and the molars M1 and M2. Similarly, the lower dentition includes i1, i2, p1, p3, p4, m1, m2, and m3.

Results and Discussion

Age class and skull shape

All specimen of our investigation are clearly subadults, which we judged by the incomplete fusion of skull bones and the incomplete eruption of the last molars. Giannini *et al*. (2006) described ontogenetic skull changes of *Pteropus* and the pattern of fusion of various skull elements and classified them into eight age stages. In all *Eidolon* specimens the *sutura interfrontalis* is completely fused, but the *sutura sagittalis* and the interparietal (except in MTDB14002) are still visible, but show first signs of a beginning fusion. So the specimens can be assigned to an age between age class 1 and 2. A comparison of the fusion pattern with *Pteropus* is not possible, due to of the lack of *Eidolon* specimens with different ages.

The skull length of MTDB14000 is 47.85 mm (measured from the rostral end of the nasals to the caudalmost point of the supraoccipital) and the rostrum length is

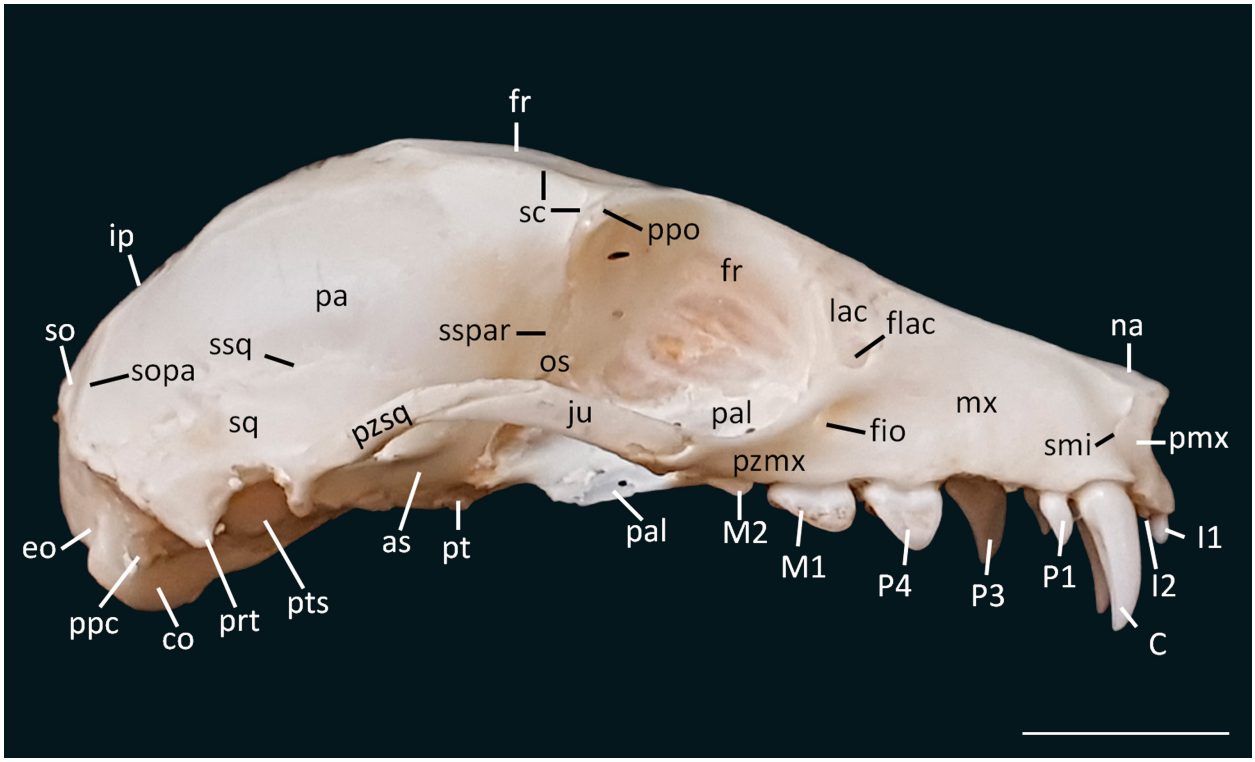

Fig. 2. Lateral view of the skull of *Eidolon helvum* (MTDB14000). Abbreviations: **as** os alisphenoidale, **C** upper caninus **, co** condyles occipitale, **eo** os exoccipitale, **fio** foramen infraorbitale, **flac** foramen lacrimale, **fr** os frontale, **I1** first upper incisvus**, I2** second upper incisvus**, ip** os interparietale, **ju** os jugale, **lac** os lacrimale, **M1** first upper molar, **M2** second upper molar, **mx** os maxillare **na** os nasale, **os** os orbitosphenoidales, **P1** first upper premolar, **P3** third upper premolar, **P4** fourth upper premolar, **pa** os parietale, **pal** os palatinum, **pmx** os incisivum, **ppc** processus paracondylaris, **ppo** processus postorbitalis,**prt** processus retrotympanicus, **pt** os pterygoideum, **pts** pars petrosa ossis temporalis, **pzmx** processus zygomaticus of maxilla, **pzsq** processus zygomaticus of squamosal, **sc** sutura coronalis, **smi** sutura maxilloincisiva, **so** os supraoccipitalis, **sopa** sutura occipitoparietalis, **sq** pars squamosal ossis temporalis, **sspar** sutura sphenoparietalis, **ssq** sutura squamosa. Scale bar = 1 cm.

16.16 mm (measured between the rostral end of the nasals and the front of the orbit; Table 2). Andersen (1912) described the rostrum proportionally longer than in *Rousettus*, but shorter and not so slender as in *Eidolon dupreanum*. The rostrum-to-skull ratio amounts to 1 : 2.96 and corresponds with the results of other studies for *Eidolon* (Springer, 1995; Romagnoli & Springer, 2000). The rostral axis, represented by the alveolar line, intersects the occiput at the supraoccipital as described in Giannini *et al*. (2006). This means that the rostral axis is deflected with respect to the basicranial axis.

The skull as a whole

Dorsal view of the skull. The rostrum comprises the nasals medially and the corpus of the maxilla laterally (Fig. 1). The zygomatic arch, consisting of the zygomatic process of the maxilla, the jugal and the zygomatic process of the squamosal, builds the most lateral part in dorsal view. Both roots form a strong triangular surface, whereby the jugal in the middle has a filigree shape.

In the rostral rim of the orbit is the lacrimal located. The long frontal is in the center of the dorsal skull and stands out with its very prominent triangular *processi postorbitalis*, which protrudes straight lateral. On the medial line of the processus root is the big *foramen postorbitalis*.

The parietal and the interparietal build the bulbous braincase, whereby the prominent *christa nuchae* marks the most caudal part in dorsal view.

Lateral view of the skull. In ventral view the small premaxilla is visible, building the apex of the viscerocranium with a dorsal contact to the nasal (Fig. 2). To the lateral rostrum belongs also the maxilla, pierced by the *foramen infraorbitale,* and the lacrimal with a lucid lacrimal foramen. The upper tooth row consists of two incisors, one canine, three premolars and two molars. Laterally, the zygomatic arch protudes with an undulating form.

The orbit is a big cavity, not quite in the center of the skull and consists of parts of the frontal with its postorbitalis process, the palatine, the lacrimal and the orbitosphenoid.

The braincase as a whole has an oval shape, with its highest point in the middle of the *sutura coronalis* of the frontal. The parietal and the squamosal build the lateral surface and the interparietal and supraoccipital seal the braincase in caudal direction. Ventrolaterally, there are parts of the following bones visible, from rostral to cau-

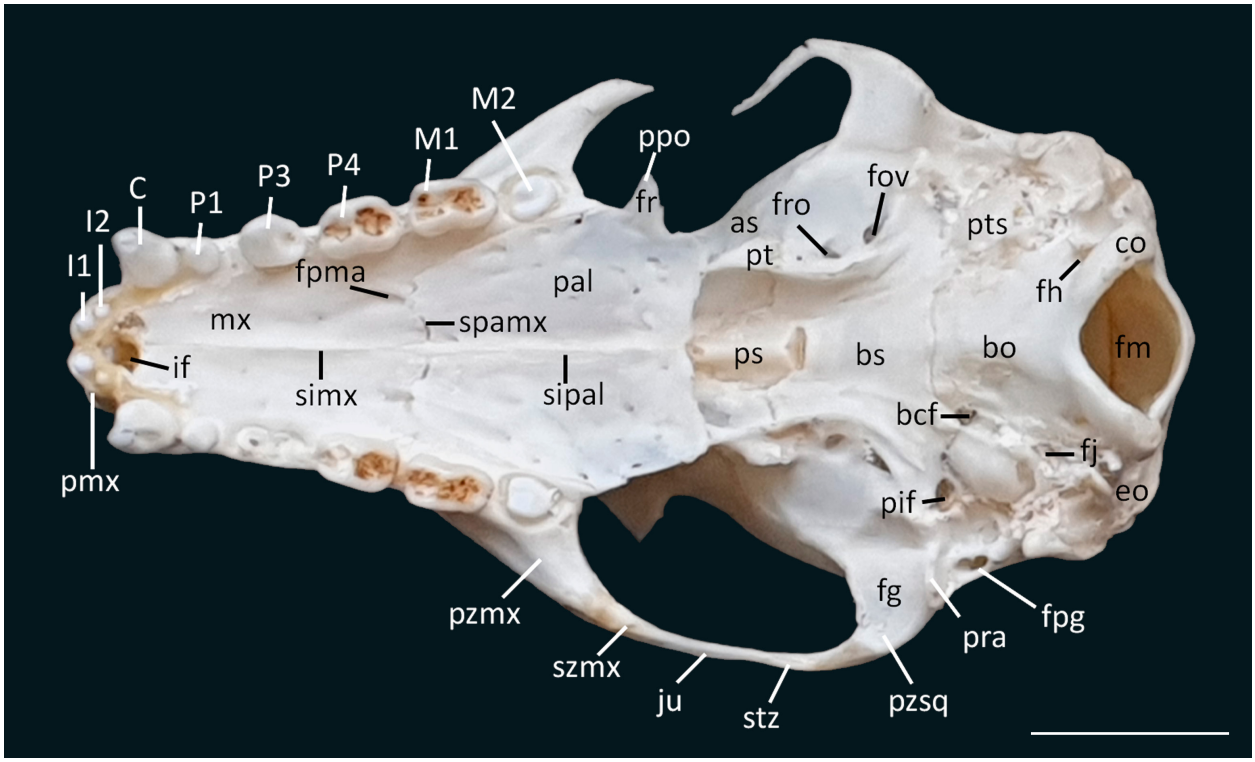

Fig. 3. Ventral view of the skull of *Eidolon helvum* (MTDB14000). Abbreviations: **as** os alisphenoidale, **bcf** basicochlear fissure, **bo** os basioccipitale, **bs** os basisphenoidale, **C** upper caninus, **co** condyles occipitale, **eo** os exoccipitale, **fg** fossa glenoidalis**, fh** foramen hypoglossi, **fj** foramen jugulare, **fm** foramen magnum, **fov** foramen ovale, **fpg** foramen postglenoidalis, **fpma** foramen palatinum majus, **fr** os frontale, **fro** foramen rotundum, **I1** first upper incisivus**, I2** second upper incisivus, **if** incisive fissure, **ju** os jugale, **M1** first upper molar, **M2** second upper molar, **mx** os maxillare, **P1** first upper premolar, **P3** third upper premolar, **P4** fourth upper premolar, **pal** os palatinum, **pif** piriform fenestra, **pmx** os incisivum, **ppo** processus postorbitalis, **pra** processus retroarticularis, **ps** os presphenoidale, **pt** os pterygoideum, **pts** pars petrosa ossis temporalis, **pzmx** processus zygomaticus of maxilla, **pzsq** processus zygomaticus of squamosal, **sipal** sutura interpalatina, **simx** sutura intermaxillaris, **spamx** sutura palatomaxillaris, **stz** sutura temperozygomatica, **szmx** sutura zygomaticomaxillaris. Scale bar = 1 cm.

dal: the palatine, the pterygoid, the alisphenoid, the petrosal and the exoccipital with the occipital condyle.

Ventral view of the skull. The rostral part of the ventral surface shows the hard palate with the palatine process of the maxilla and the *lamina horizontalis* of the palatine. Rostral of the canines are the premaxillae located, which surround the huge *foramen incisivum* (Fig. 3). The caudal edge of the palatine is free and contacts the pterygoid. The nasypharyngeal region contributes medially the presphenoid and the basisphenoid and laterally the pterygoid and the alisphenoid. The ali- and basisphenoid is pierced by two prominent foramina: the *foramen ovale* and *foramen rotundum*. The medial surface of the caudal skull is built by the wide basioccipital, which leads caudally to the large *foramen magnum* with the protruding occipital condyles (Fig. 9). Lateral of the basioccipital is the petrosal with the conspicuous rounded promontorium. The petrosal, as well as the ectotympanic and alisphenoid surround a large opening: the piriform fenestra. The ventral side of the zygomatic arch is the most lateral part the skull.

Occipital view of the skull. The ventral part of the occiput is built by the exoccipital and the occipital condyles with the lateral *processi paracondylaris*. The large supraoccipital is divided by the prominent horizontal *christa nuchae* and vertical *christa occipitalis externa* (Fig. 4). Dorsal of the supraoccipital is the single, triangular interparietal situated. The parietal occupies the dorsal and lateral braincase with a smooth surface.

The skull bones

Rostral bones

Nasal: The nasal (*os nasale*) is a flat paired bone that builds the roof of the *cavum nasi* and expands from the level of P4 to its apex, which ends with a free margin. It articulates anteroventrally with the premaxilla, forming a short *sutura nasoincisiva*, caudally with the frontal, forming an arched *sutura frontonasalis* and laterally with the maxilla, forming a slightly medially curved *sutura nasomaxillaris*.

The two nasals are connected by the *sutura internasalis* (Fig. 1), which appears straight and plane from the apex to the frontal. The rostral apex forms the dorsal external opening of the nose, but with a smaller overhang than the ventrally proportion of the premaxilla.

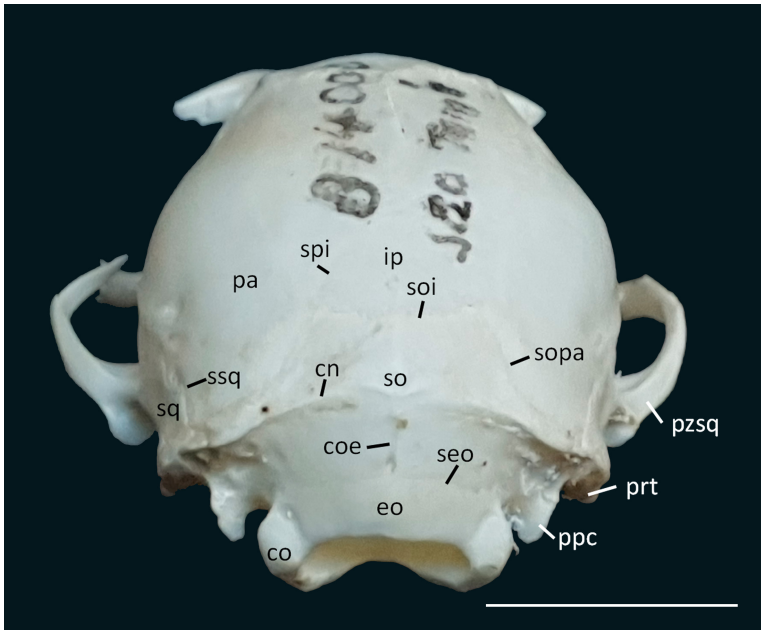

Fig. 4. Occipital view of the skull of *Eidolon helvum* (MTDB14000). Abbreviations: **cn** crista nuchae, **co** condylus occipitalis, **coe** crista occipitalis externa, **eo** os exoccipitale, **ip** os interparietale, **pa** os parietale, **ppc** processus paracondylaris, **prt** processus retrotympanicus, **pzsq** processus zygomaticus of squamosal, **seo** sutura between ex- and supraoccipitalis, **so** os supraoccipitale, **soi** sutura occipitointerparietalis, **sopa** sutura occipitoparietalis, **spi** sutura parietointerparietalis, **sq** pars sqamosal ossis temporalis, **ssq** sutura squamosa. Scale bar = 1 cm.

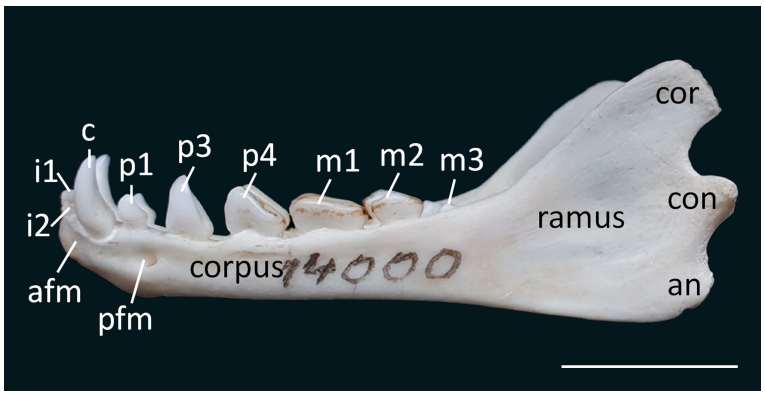

Fig. 5. Lateral view of left mandible of *Eidolon helvum* (MTDB14000). Abbreviations: **afm** anterior foramen mentale, **an** angulus mandibularis, **c** lower caninus, **con** processus condylaris, **cor** processus coronoideus, **i1** first lower incisivus, **i2** second lower incisivus, **m1** first lower molar, **m2** second lower molar, **m3** third lower molar, **p1** first lower premolar, **p3** third lower premolar, **p4** fourth lower premolar, **pfm** posterior foramen mentale. Scale bar = 1 cm.

Premaxilla. The premaxilla (*os incisivum*) is a small paired bone, which forms the apex of the viscerocranium and articulates posteriorly with the maxilla, forming the *sutura maxilloincisiva* (Fig. 2), and dorsally with the nasal, forming the *sutura nasoincisiva*. It compromises two osseous parts: the *corpus ossis incisive* and the *processus nasalis*. The premaxillary shape is very similar to those of *Rousettus* and *Boneia* (ANDERSEN, 1912).

The contact zone between the right and left premaxilla is short (*sutura interincisiva*) and each bone includes the alveoli for two incisors (I1 and I2).

The ventral part of the premaxilla extends rostroventrally, so there is no contact between premaxilla and maxilla at this point and it also forms a diastema between I2 and C. The distinct separation of the premaxillaries in front (only connected by fibrous tissue) is also to be found in other Pteropodidae like *Boneia* and occasionally in *Eonycteris* and *Melonycteris* (ANDERSEN, 1912).

In ventral view, a marked incisive fissure is visible (Fig. 6), which is surrounded by both premaxillary bones and the anterior part of the *processus palatinus* of the maxilla. Like in *Pteropus,* the fissure is formed by the converging paired incisive foramina (GIANNINI *et al*., 2006).

Maxilla. The maxilla (*os maxillare*) is a paired bone, which together with the premaxilla forms the upper jaw. There are three main structures to describe: a body (*corpus maxillae*), an alveolar surface (*processus alveolaris*) and a palatine process (*processus palatinus*).

The *corpus maxillae* has a long surface and is located on the lateral part of the rostrum. Rostrally, it contacts the premaxilla (*sutura maxilloincisiva*), the nasal dorsally (*sutura nasomaxillaris*), the lacrimal posteriorly (*sutura lacrimomaxillaris*) and there is only a small posterior contact zone to the frontal. The zygomatic process of the maxilla contacts posteriolly the jugal, forming the *sutura zygomaticomaxillaris*. Dorsal of the alveolar surface (*processus alveolaris*), at the level of M1, *the canalis infraorbitalis* opens rostral with the *foramen infraorbitale* (Fig. 7).

The alveolar surface has a free margin (*margo alveolaris*) and compromises the alveoli for two incisors (I1, I2), one canine (C), three premolars (P1, P3, P4) and two molars (M1, M2). In comparison to *Pteropus*, the P1 is much larger (GIANNINI *et al*., 2006).

The palatine process (*processus palatinus*) protrudes as a transverse bony plate medially and articulates with

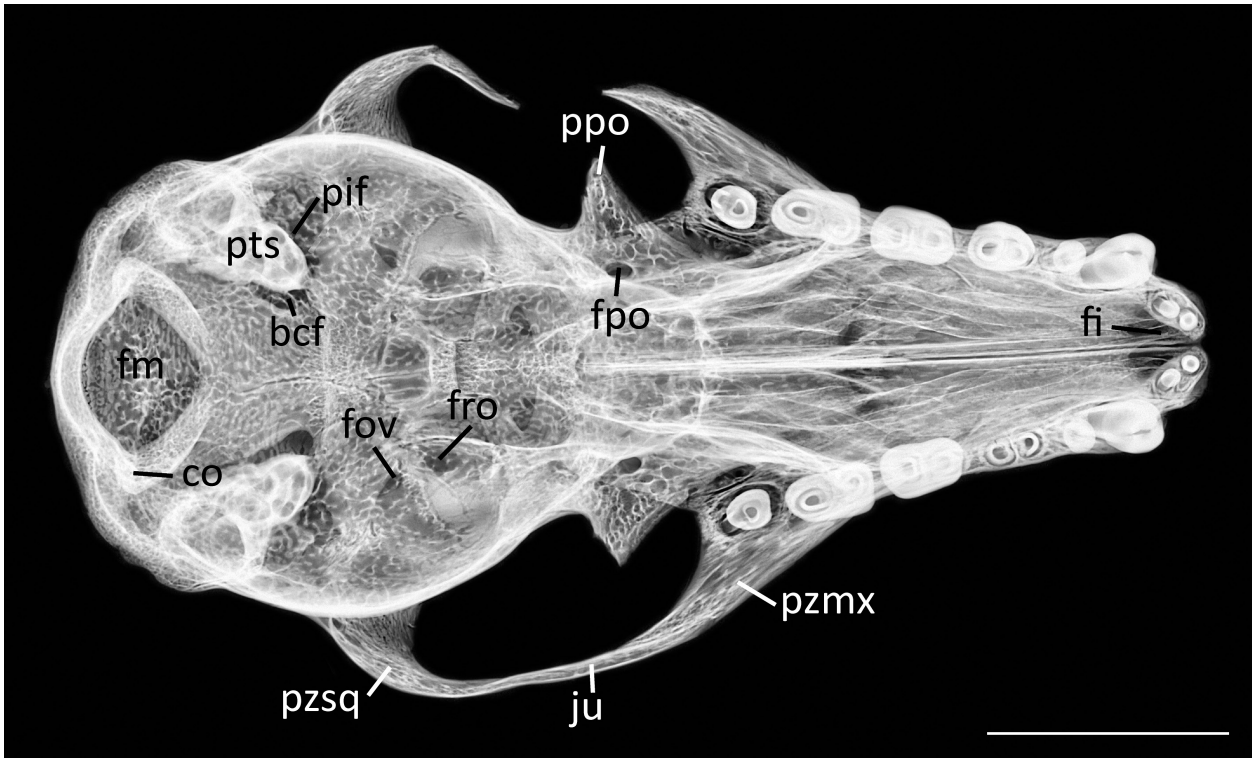

Fig. 6. Radiograph of dorsoventral view of the skull of *Eidolon helvum* (MTDB14000). Abbreviations: **bcf** basicochlear fissure, **co** condylus occipitalis, **fi** foramen incisivum, **fm** foramen magnum, **fo** foramen ovale, **fpo** foramen postorbitale, **fro** foramen rotundum, **ju** os jugale, **pif** piriform fenestra, **ppo** processus postorbitalis, **pts** pars petrosa ossis temporalis, **pzmx** processus zygomaticus of maxilla, **pzsq** processus zygomaticus of squamosal. Scale bar = 1 cm.

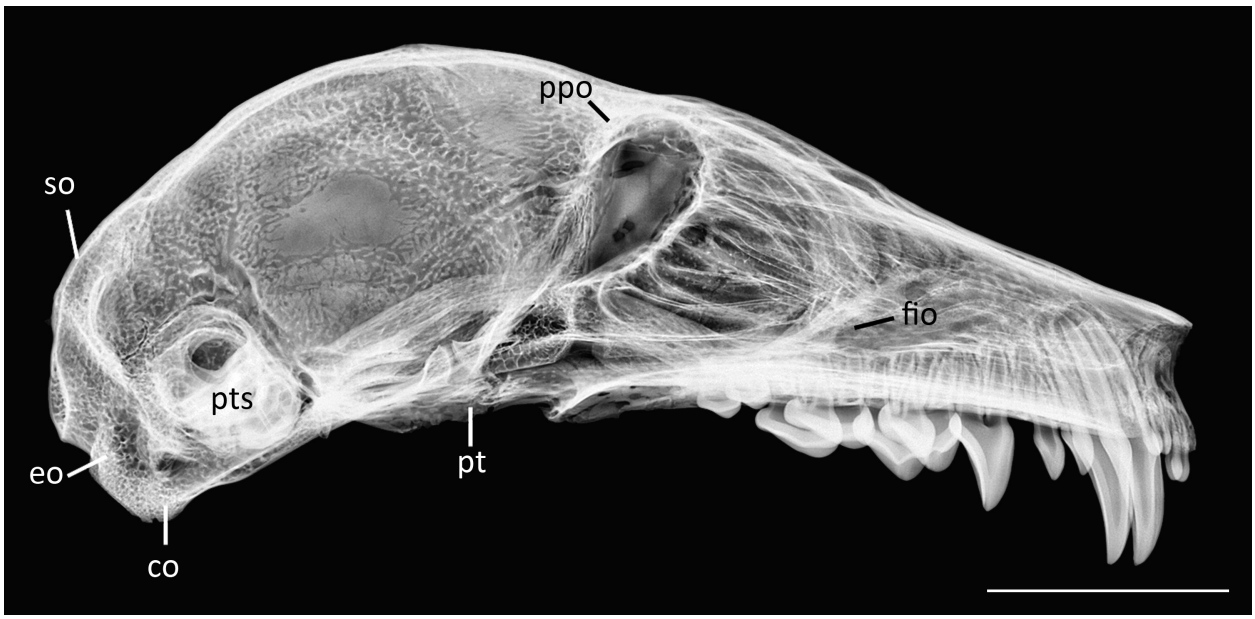

Fig. 7. Radiograph of lateral view of the skull *Eidolon helvum* (MTDB14000). Abbreviations: **co** condylus occipitalis, **eo** os exoccipitalis, **fio** foramen infraorbitale, **ppo** processus postorbitalis, **pt** os pterygoideum, **pts** pars petrosa ossis temporalis, **so** os supraoccipitalis. Scale bar = 1 cm.

the maxilla of the opposite side along the midsagittal line in the anterior palate, forming the slightly raised *sutura intermaxillaris* (Fig. 8), which extend from the anterior part of the *processus palatinus* to the level of P4 and M1. The posterior part of the processus connects with the palatine, forming the *sutura palatomaxillaris*, starting laterally at the level of M3 and ending medially at the level between P4 and M1. Directly in front of the margin of this suture is the *foramen palatinum majus* (both sides) located. Originating from the foramen, the *sulcus palati-*

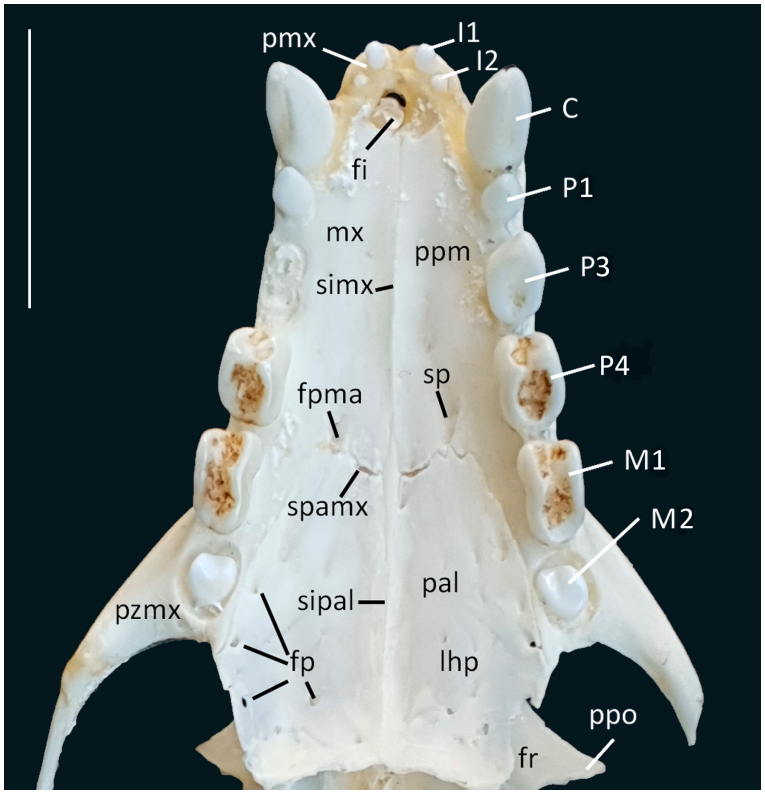

Fig. 8. *Eidolon helvum* (MTDB14000) in ventral view of hard palate. Abbreviations: **C** upper caninus, **fi** foramen incisivum, **fp** series of foramina palatina, **fpma** foramen palatinum majus, **fr** os frontale, **I1** first upper incisivus**, I2** second upper incisivus, **lhp** lamina horizontalis of palatine, **M1** first upper molar, **M2** second upper molar, **M3** third upper molar, **mx** os maxillare, **P3** third upper premolar, **P4** fourth upper premolar, **pal** os palatine, **ppm** processus palatinus of maxilla, **pmx** oc incisivum, **ppo** processus postorbitalis, **pzmx** processus zygomaticus of maxilla, **simx** sutura intermaxillaris, **sipal** sutura interpalatina, **sp** sulcus palatinus, **spamx** sutura palatomaxillaris. Scale bar = 1 cm.

nus extends from here anteriorly and ends at the level of P4.

Palatine. The palatine (*os palatinum*) is a paired bone and consists of two laminae: the *lamina horizontalis* and *lamina perpendicularis*. The *lamina horizontalis* forms the caudal end of the hard palate and contacts rostrally the palatine process of the maxilla (*sutura palatomaxillaris*). The caudal part is free and the bone of the lateral edge is considerable thin. In *Pteropus lylei* the caudal edge is described as deeply concave and the margin is more straight (Giannini *et al*., 2006), while in *E. helvum* the margin is irregularly serrated and forms only a slight concave bow (Figs 3, 8).

The caudal and lateral margins are building a caudal angle, which contacts the pterygoid.

The *sutura interpalatina* separates both *laminae horizontalis* and is an extension of the *sutura intermaxillaris* (which is part of the *sutura palatina mediana* in the NAV; Figs 3, 8). It appears slightly raised, while Giannini *et al*., (2006) described it in *P. lylei* as straight and plane. A series of clear foramina is located on the lateral rim of the caudal edge of the horizontal lamina, whereby the foramina along the molars are more inconspicuous.

The *lamina perpendicularis* articulates the frontal dorsally, forming the *sutura frontopalatina*, which appears irregularly curved. The anterodorsal contact to the lacrimal (*sutura palatolacrimalis*) is very short (1–2 mm) and somehow more a contact point than a suture. The *lamina perpendicularis* contacts the maxilla rostrally (suture described above), the presphenoid dorsomedially (*sutura sphenopalatina*) and the pterygoid caudally (*sutura pterygopalatine*). In *Pteropus lylei*, the caudomedial edge of the palatine is separated by a vacuity (*fissura pterygopalatine*; Giannini *et al*., 2006), but in *Eidolon helvum* there is no gap between these two bones.

Lacrimal. The lacrimal (*os lacrimale*) is a small, paired bone, situated on the rostral rim of the orbit. The *crista orbitalis* can be divided into two surfaces: *facies orbitalis* and *facies facialis*, whereby the larger *facies facialis* is on the dorsal surface and the much smaller *facies orbitalis* is part of the orbit. The lacrimal articulates with the maxilla rostrally and ventrally (*sutura lacrimomaxillaris*), the frontal dorsally and caudally (*sutura frontolacrimalis*) and the palatine caudally (*sutura palatolacrimalis*). Within the *facies facialis* is the major *foramen lacrimale* located (Fig. 2), the entrance of the internal lacrimal canal (*canalis lacrimalis*). The ventral margin of the foramen is built by the maxilla and dorsocaudally the lacrimal forms a pronounced pit for the lacrimal sac (*fossa sacci lacrimalis*).

Jugal. The jugal bone (*os zygomaticum, os jugale*) is a small, paired bone and forms the middle part of the zygomatic arch. It is embedded between the maxilla and the squamosal (suture described above). The *processus temporalis* of the jugal has a long articulation with the squamosal (*sutura temporozygomatica*; Fig. 3). Laterally as well as medially, this suture has a diagonal course from dorsal to ventral. The articulation of the processus maxillaris of the jugal with the maxilla is shorter and more compact.

The corpus of the jugal has two margins, the rostral *margo massetericus* and the caudodorsal *margo infraorbitalis*, and also two surfaces (*facies lateralis* and *facies orbitalis*).

Cranial bones

Frontal. The frontal (*os frontale*) is a large, paired bone, which forms the rostral skullcap (*squama frontalis*) and also the bulk of the orbit (*pars orbitalis*). The preorbital proportion (*pars nasalis*) is short and the frontal articulates here with the lacrimal (*sutura frontolacrimalis*), the maxilla (*sutura frontomaxillaris*) and the nasal (*sutura frontonasalis*). In MTDB14000 the interfrontal suture (*sutura interfrontalis*) between both frontals is almost completely fused; only in the rostral area the midsagittal line is visible. The concave *pars orbitalis* forms most of the eye socket wall, whereby the bone structure is obviously thin and the *sinus frontalis* is visible, which is also to recognize in the lateral X-ray image (Fig. 7). There are contacts to three other bones: the palatine ventrally (*sutura frontopalatina*), the lacrimal rostrally (*sutura frontolacrimalis*) and the orbitosphenoid caudally (*sutura sphenofrontalis*). Dorsal to the orbit is the very prominent *processus postorbitalis* located. With a triangular form, the process extends straight laterally and builds a kind of a roof over the posterior eye socket. It towers the orbit by 3.29 mm in MTDB14000 und thus, it is more pronounced as in the studied *Pteropus lylei* specimen in Giannini *et al*. (2006). Caudal to the postorbital process is the *sutura coronalis*, whitch runs in dorsal direction, then straight caudally and then turns medially in a right angle, till it meets the counterpart at the midsagittal line. The *sutura coronalis* separates the frontal from the parietal.

In the middle of the medial line of the root of the postorbital process is the large *foramen postorbitale* situated (Fig. 1). The foramen perforates the bone completely and opens on the ventral side medial of the *processus postorbitalis* by forming a deep caudoventral sulcus.

Parietal. The paired parietal (*os parietale*) is an element of the neurocranium and builds the major part of the dorsal and lateral skull roof. Rostrodorsally, both parietals border the frontal with the *sutura coronalis* (see descriptin above) and meet each other through the sagittal suture (*sutura sagittalis*), which is completely flat and gets indistinct in caudal direction (Fig. 1), while *Desmodus rotundus* shows a low sagittal crest (Reyes-Amaya & Jerez, 2013) . The *sutura sphenoparietalis* attaches rostrolaterally the parietal with the orbitosphenoid and anteroventrally with the alisphenoid. The contact zone to the squamosal passes ventrolaterally (*sutura squamosa*) and caudally the parietal is bordered by the interparietal (*sutura parietointerparietalis*) and supraoccipital (*sutura occipitoparietalis*). The foramina for rami temporalis (term found by Giannini *et al*., 2006) are situated dorsal of the *sutura squamosal*. The expression of these vary: in specimen MTDB1400 they appear as two foramina on the left side. On the right side is only one opening clearly visible and our other specimens exhibit no foramina at all. This could mean that the supply of the *musculus temporalis* has been taken over completely by a lateral, extracranial larger vessel of the carotid artery. Or it could be related to environmental or genetic stress during ontogenesis (Tomkins & Kotiaho, 2001), which can manifest in fluctuating asymmetry as an indicator of the developmental stability of populations (Zakharov *et al*., 1991; Badyaev *et al*., 2000; Ansorge, 2001; Wójcik *et al*., 2007).

Interparietal. The interparietal (*os interparietale*) is a triangular, unpaired bone between the parietal and supraoccipital on the mediocaudal skull roof. The mediocaudal *sutura occipitointerparietalis* is clearly visible and slightly serrated (Fig. 4). The *sutura parietointerparietalis* is more squamous and the first signs of a fusion between parietal and interparietal can be observed here. Both sutures meet caudally at a point where parietal, interparietal and supraoccipital meet each other. From here the parietointerparietal suture runs in dorsorostral direction to the midsagittal line, where it merges with its counterpart. The surface of the interparietal is very smooth and no foramina are visible.

Pterygoid. The pterygoid (*os pterygoideum*) is a paired bone situated ventral to the sphenoid complex and caudal to the palatine. It appears as a small ventral lamina with two surfaces: the lateral *facies pterygopalatina* and the medial *facies nasopharyngea*. The latter articulates rostrally with the palatine, mediorostrally with the presphenoid and medially with the basisphenoid (all sutures described above). The *facies pterygopalatine* is smaller and there is no clear suture visible to define the pterygoid from the basi-alisphenoid complex. The *sutura pterygopalatina* appears very irregular, whereby a described gap between both bones in *Pteropus lylei* (Giannini *et al*., 2006) is not to be found. Both *facies* meet each other at a ventral margin, which has a low medial *hamulus pterygoideus* (Fig. 9).

Sphenoidal complex. The sphenoidal complex forms the rostral part of the basicranium and comprises four elements: the both unpaired *os presphenoidale* and *os basisphenoidale* and the both paired bones *ossa alisphenoidales* and *ossa orbitosphenoidales*.

The presphenoid is visible in ventral view as a small, rhomboid bone and is situated between the palatine (rostrolaterally; *sutura sphenopalatina*) and the pterygoid (caudolaterally; *sutura pterygosphenoidalis*). The surface is pervaded through an obvious raised midsagittal crest, the *crista sphenoidalis* (Fig. 9), which spreads in caudal direction. The space between pre- and basisphenoid corresponds with the loss of interlocking cartilage (the intersphenoidal synchondrosis) as observed in one *Pteropus lylei*-specimen (Giannini *et al*., 2006).

The basisphenoid is embedded with its triangular shape between the presphenoid, alisphenoid and pterygoid (Figs 3, 9). Laterally the basisphenoid is bordered

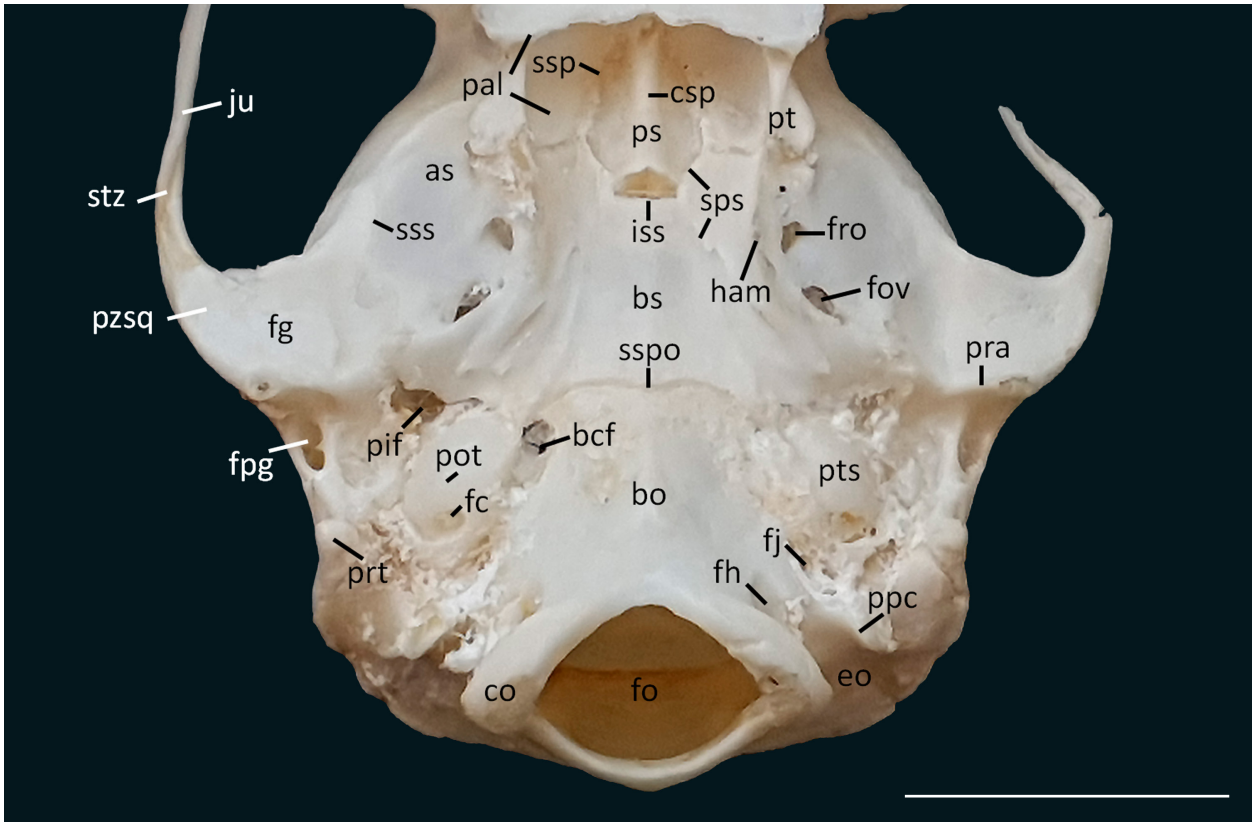

Fig. 9. *Eidolon helvum* (MTDB14000)´in ventral view of the nasopharyngeal and occipital region. Abbreviations: **as** os alisphenoidale, **bcf** basicochlear fissure, **bo** os basioccipitale, **bs** os basisphenoidale, **co** condyles occipitale, **csp** crista sphenoidalis, **eo** os exoccipitale, **fc** fenestra cochlea, **fg** fossa glenoidalis**, fh** foramen hypoglossi, **fj** foramen jugulare, **fm** foramen magnum, **fov** foramen ovale, **fpg** foramen postglenoidalis, **fro** foramen rotundum, **ham** hamulus pterygoideus, **iss** intersphenoidal synchondrosis, **ju** os jugale, **pal** os palatinum, **pif** piriform fenestra, **pot** promontorium, **ppc** processus paracondylaris, **pra** processus retroarticularis, **prt** processus retrotympanicus, **ps** os presphenoidale, **pt** os pterygoideum, **pts** pars petrosa ossis temporalis, **pzsq** processus zygomaticus of squamosal, **sps** sutura pterygpsphenoidalis, **ssp** sutura sphenopalatina, **sspo** synchondrosis sphenooccipitalis, **sss** sutura sphenosquamosa, **stz** sutura temperozygomatica. Scale bar = 1 cm.

by the pterygoid (*sutura pterygosphenoidalis*) and the ventral surface enlarges in caudolateral direction and fuses with the alisphenoid, but it is no clear suture visible. The caudal border with the basioccipital is curved, where a missing cartilage is placed, the *synchondrosis sphenooccipitalis*.

The caudal part of the alisphenoid is situated laterally of the basisphenoid. It spreads like a wedge in rostrodorsal direction, where both rims of the alisphenoid merge in a tip like endpoint that articulates with the orbitosphenoid. Rostrodorsally, the *sutura sphenoparietalis* appears straight and separates the parietal from the overlapping alisphenoid. Caudolaterally, the squamosal overlaps the alipshenoid forming the *sutura sphenosquamosa*. Two prominent foramina are present: the *foramen ovale* and *foramen rotundum* (Figs 3, 9). The outer rims of the caudal *foramen ovale* are formed by the alisphenoid and basisphenoid, but because the bones are fused, no clear allocation is possible. This also applies to the rostral *foramen rotundum* which is embedded in the alisphenoid and pterygoid. In contrast, some species show different conditions of these foramina. For example, *Pteropus tonganus* and *P. admiralitatum* as well as many other pteropodines have also two separated foramina, while in some *Pteropus* species, it appears only as one large opening. GIANNINI *et al*. (2006) identified it for *P. lylei* as the alisphenoid foramen confluent with the *foramen ovale*.

In *Eidolon*, another large opening appears on the caudolateral margin of the alisphenoid, the piriform fenestra, which caudal rim is contributed by the petrosal.

The orbitosphenoid is a fragile, triangular structure and forms the caudal part of the orbit (Fig. 2). It contacts the parietal dorsocaudally, the frontal rostrally and the alisphenoid ventrocaudally (see description above) and parts of the surface of the orbitosphenoid are overlapped by all of these three bones. In the base is the very prominent *canalis opticus* situated. The orbitosphenoid and alisphenoid are located in the infratemporal fossa.

Squamosal. The squamosal (*Os temporale*, *pars squamosal*) is a paired, lateral bone of the braincase and consists of a flattened squama and a prominent rostrolateral zygomatic process (*processus zygomaticus*), which is the posterior part of the zygomatic arch (Fig. 2). The root of the process is characterized by a horizontal triangular shape. The ventral side of the root comprises the glenoid

fossa (*fossa glenoidalis*), which articulates with the mandible, forming the *articulatio temperomandibularis* and is bordered caudally by the *processus retroarticularis* (Figs 3, 9). The depression on the dorsal side is an origin area for the *musculus temporalis*. Directly caudal of the *processus retroarticularis* appears the *foramen postglenoidalis* as a large and oval opening. Originating from the root, the process runs as a thin compressed bone in rostrodorsal direction till it joins with the jugal (suture described above), whereby the ventral margin is quite narrower than the dorsal opposite side.

The squamosal articulates with the parietal dorsally (suture described above), with the alisphenoid rostroventrally (*sutura sphenosquamosa*) and with the petrosal caudally and laterally (*sutura squamosomastoidea*). The squama overlaps all of these three bones, which is clearly visible at specimen MTDB14001.

Petrosal. The paired petrosal (*os temporale, pars petrosa*) is part of the basicranium (Figs 6, 7) that contains the organs of hearing and equilibration. The bone can be divided into two structures: the anteroventromedial *pars cochlearis* and the more posterodorsal and lateral *pars canalicularis*. Most parts of the petrosal are not easily to study without isolating them, so we focus here on the accessible structures. On the ventral skull side the petrosal has a prominent dome-shaped promontorium (Fig. 9). It is longer than wide and anteromedially the curvature is flatter than on the opposite side. Especially noticeable is the medial border of the promotorium, which is defined by a rough margin. Like in *Pteropus lylei* (Giannini *et al*., 2006) there are two apertures on the outer edge of the promontorium: the caudal *fenestra cochlea* and the caudolateral *fenestra vestibuli*. Anteromedially, the petrosal has a point contact to the basisphenoid. Anterolaterally it contacts the alisphenoid, laterally the ectotympanic, medially the basioccitpital and caudally the exoccipital (*sutura occipitomastoidea*).

In the X-ray images the petrosal is well definable as a slightly oval bone (Figs 6, 7).

Ectotympanic. The ectotympanic (*annulus tympanicus*) is situated laterally of the petrosal and caudally of the piriform fenestra. It appears wide and forms a short bony auditory meatus and is one of the prominent peculiarities of *Eidolon*, because in all other bats the ectotympanic is annular (Andersen, 1912). In *Pteropus* the bone has an elliptic shape (Giannini *et al*., 2006) and in *Roussettus* it is also typically ring-like and even broader than in most other genera (Andersen, 1912).

Occipital complex. The occipital complex (*os occipitale*) comprises three parts: an upaired basioccipital, an unpaired supraoccipital and a paired exoccipital. They all surround the oval shaped *foramen magnum* (Fig. 6).

Basioccipital: The basioccipital is situated on the ventral side of the skull and a straight perpendicular margin devides the ventral surface into two parts (Fig. 9). Rostrally, a vertical, slightly curved synchondrosis separates the bone from the basisphenoid. The synchondrosis meets laterally the petrosal and caudally has contact to the basicochlear fissure. The rostrolateral rim of the basioccipital articulates with the petrosal and caudolateral with the exoccipital, but the synchondrosis are seamlessly fused. The caudal margin of the basioccipital is simultaneously the ventral concave margin of the foramen magnum, which is open ventrocaudally.

Exoccipital: On the ventral side, the paired exoccipital is situated posterolateral to the basioccipital and extends lateral to the *foramen magnum* on the occipital side. Two foramina are situated on the ventral side: the *foramen jugulare* caudomedial of the petrosal and the *foramen hypoglossi* on the rostral edge of the occipital condyles (Figs 3, 9). No sutures are visible, so the clear bone belonging of the foramina is difficult. The *processus paracondylaris* appears as a prominent feature lateral of the hypoglossal foramen. Lateral of the *foramen magnum* are the *condyli occipitales* situated, which are the cranial articular joints of the *articulatio atlantooccipitalis*. The border between ex- and supraoccipital is characterized through a horizontal suture that passes from one dorsal end of the condyles occipitalis to the other. So the exoccpital participates in the dorsal margin of the *foramen magnum* (Fig. 4).

Supraoccipital: The supraocciptal forms the dorsal part of the occiput. It contacts dorsomedially the interparietal, dorsolaterally the parietal, ventrolaterally the petrosal and ventromedially the exoccipital (see describtion above). The prominent *crista nuchae* passes semicircular and separates the bone in two even ventral and dorsal parts (Fig. 4). From the *sutura occipitointerparietalis* to the *foramen magnum* runs another significant median crest, the *crista occipitalis externa*.

Mandible. The paired mandible (*mandibula*) comprises two parts: the horizontal rostral *corpus mandibulae* and the caudal *ramus mandibulae*. Anteriorly both mandibles are completely fused at the *symphysis mandibulae*. The corpus is laterally flattened and has three surfaces: *facies lingualis*, *facies buccalis* and *facies labialis*. The alveolar surface contains the alveoli for two incisors (i1, i2), one canine (c), three premolars (p1, p3, p4) and three molars (m1, m2, m3). There are two small diastemata between p1 and p3 and between p3 and p4 to notice. Two foramina are clearly visible, the posterior *foramen mentale* on the *facies buccalis* on the level between p1 and p3 and the *facies labialis* bears the anterior *foramen mentale* ventral to i1 and i2 (Fig. 5). The caudal third of the mandible belongs to the *ramus mandibulae*, a thin, flat bone plate. Markedly, the dorsal margin is a continuation of the alveolar margin and rises in a angle 45 degree, beginning about 3 mm posterior to m3, while in *P. lylei* the increase starts immediately caudal of the last molar (Giannini *et al*., 2006). The lateral surface is even and in the middle is the *fossa masseterica* located. The caudal end is characterized by two processi: the *processus coronoideus* and the *processus condylaris*, which are separated through a distinct kind of notch (*incisura mandibulae*). Giannini *et al*. (2006) described for *Pteropus lylei* that

the maximum height of the coronoid process is equivalent to the height of the canine, but in *Eidolon helvum* specimen MTDB14000, the coronoid hight is quite higher (14.05 mm). The *processus condylaris* is in the middle of the caudal border of the ramus and builds the inferior joint surface of the *articulatio temperomandibularis*. The caudoventral *angulus mandibularis* is unobtrusive. The medial surface of the ramus is divided through a horizontal crest, which reaches from the *processus condylaris* to the posterior end of m3. Ventral of this crest, in the middle of the medial surface, is the well pronounced *foramen mandibularis* with a clearly visible sulcus caudally.

Conclusions

With this study we have given a basic morphological description of the skull of the pteropodid bat *Eidolon helvum*. We are aware of the fact that the main description is based on few specimens, all subadults so that statements on ontogenetic development are not possible. The study reveals similarities and differences to *Pteropus* and other bats. The two prominent characters of *Eidolon* are the large P1 and the very unique peculiarity of the ectotympanic, which appears as a short bony auditoy meatus. Also the palatine shows some differences like the *processus postorbitalis* is more pronounced in *E. helvum*, the *sutura interpalatine* is more raised, the caudal edge of the palatine is more irregular serrated and forms only a slight concave bow; there is no vacuity in the caudiomedial margin of the palatine and also no gap to the pterygoid. *E. helvum* has also a more pronounced *processus postorbitalis* and the coronoid is higher. In contrast, the premaxilla is very similar to those of *Rousettus* and *Boneia*.

As Giannini *et al*. (2006) already stated, more morphological studies are needed in bats. More advanced techniques than X-ray used here, which still failed to render fused bone sutures more visible than by sight, might help in future to describe individual bones of bats better.

Acknowledgements

We thank Mario Richter (SNSD) for his help and support with the radiography. The study was partially financially supported by Leibniz Association, SAW-2016-SGN-2. The reviewers' comments helped to improve the manuscript and are thankfully acknowledged.

References

Almeida, F. C., Giannini, N. P., Desalle, R. & Simmons, N. B. (2011). Evolutionary relationships of the Old World fruit bats (Chiroptera, Pteropodidae): Another star phylogeny? *BMC Evolutionary Biology*, **11**, 1–17.

Andersen, K. (1912). *Catalogue of the Chiroptera in the collection of the British Museum Volume I: Megachiroptera*. London, Trustees of the British Museum (Natural History).

Ansorge, H. (2001). Assessing non-metric skeleton characters as a morphological tool. *Zoology*, **104**, 268–277.

Badyaev, A.V., Foresman, K. R. & Fernandes, M. V. (2000). Stress and developmental stability: vegetation removal causes increased fluctuating asymmetry in shrews. *Ecology*, **81**, 336–345.

Bergmans, W. (1997). Taxonomy and biogeographyof African fruit bats (Mammalia, Megachiroptera). 5. The genera *Ussonycteris* Andersen, 1912, *Myonycteris* Matschie, 1899 and *Megaloglossus* Pagenstecher, 1885; general remarks and conclusions; annex: key to all species. *Beaufortia*, **47**, 11–90.

Bhatnagar, K. P. & Kallen, F. C. (1974). Cribriform plate of ethmoid, olfactory bulb and olfactory acuity in forty species of bats. *Journal of Morphology*, **142**, 71–90.

Budinski, I., Jojić, V., Jovanović, V. M., Bjelić-Čabrilo, O., Panović, M. & Vujošević, M. (2015). Cranial variation of the greater horseshoe bat *Rhinolophus ferrumequinum* (Chiroptera: Rhinolophidae) from the central Balkan. *Zoologischer Anzeiger*, **254**, 8–14.

Cooper-Bohannon, R., Mickleburgh, S., Hutson, A.M., Bergmans, W., Fahr, J. & Racey, P.A. (2020). *Eidolon helvum*. The IUCN Red List of Threatened Species 2020: e.T7084A22028026. https://dx.doi.org/10.2305/IUCN.UK.2020-2.RLTS.T7084A22028026.en.

Demos, T. C., Webala, P. W., Goodman, S. M., Kerbis Peterhans, J. C., Bartonjo, M. & Patterson, B. D. (2019). Molecular phylogenetics of the African horseshoe bats (Chiroptera: Rhinolophidae): expanded geographic and taxonomic sampling of the Afrotropics. *BMC Evolutionary Biology*, **19**, 1–14.

Drysdale, R. (2001). Phenotypic data in FlyBase. *Briefings in Bioinformatics*, **2**, 68–80.

Giannini, N. P. & Simmons, N. B. (2005). Conflict and congruence in a combined DNA–morphology analysis of megachiropteran bat relationships (Mammalia: Chiroptera: Pteropodidae). *Cladistics*, **21**, 411–437.

Giannini, N. P. & Simmons N. B. (2007). Element homology and the evolution of dental formulae in megachiropteran bats (Mammalia: Chiroptera: Pteropodidae). *American Museum Novitates* **2007**, 1–27.

Giannini, N. P., Wible, J. R. & Simmons, N. B. (2006). On the cranial osteology of Chiroptera. I. *Pteropus* (Megachiroptera: Pteropodidae). *Bulletin of the American Museum of Natural History*, **295**, 1–134.

Gkoutos, G. V., Green, E. C. J., Mallon, A.-M., Blake, A., Grennaway, S., Hancock, J. M. & Davidson, D. (2004). Ontologies for the description of mouse phenotypes. *Comparative and Functional Genomics*, **5**, 545–551.

Hiller, M., Schaar, B. T., Indjeian, V. B., Kingsley, D. M., Hagey, L. R. & Bejerano, G. (2012). A "forward genomics" approach links genotype to phenotype using independent phenotypic losses among related species. *Cell Reports*, **2**, 817–823.

Hiller, M., Ansorge, H., Chavakis, T., Fickel, J., Giere, P., Grobe, P., Hampe, J., Lehmann, T., Ortmann, S., Ruf, I., Stefen, C., Tanaka, E., Vogt, L. & Stuckas, H. (2016). Discovering the genomic basis of morphological and physiological differences between mammalian species with Forward Genomics. *Mammalian Biology*, **81**, 9–10.

Hurtado, N., & D'elía, G. (2018). Taxonomy of the genus *Gardnerycteris* (Chiroptera: Phyllostomidae). *Acta Chiropterologica*, **20**, 99–115.

Jojić, V., Budinski, I., Blagojević, J. & Vujošević, M. (2015). Mandibular and cranial modularity in the greater horseshoe bat *Rhinolophus ferrumequinum* (Chiroptera: Rhinolophidae). *Hystrix*, **26**, 163–165.

Juste, J., López-Gonzáles, C. & Strauss, R. E. (2001). Analysis of asymmetries in the African fruit bats *Eidolon helvum* and *Rousettus egyptiacus* (Mammalia: Megachiroptera) from the islands of the Gulf of Guinea. I. Variance and size components

of bilateral variation. *Journal of Evolutionary Biology*, **14**, 663–671.

Kämper, R. & Schmidt, U. (1977). Die Morphologie der Nasenhöhle bei einigen neotropischen Chiropteren. *Zoomorpholgie*, **87**, 3–19.

Laureiro, L. O., Lim, B. K. & Engstrom, M. D. (2018). A new species of mastiff bat (Chiroptera, Molossidae, *Molossus*) from Guyana and Ecuador. *Mammalian Biology*, **90**, 10–21.

Lee, J. H. & Hiller, M. (2017). Genome-wide screens for molecular convergent evolution in mammals, (pp. 297–312) *in*: Pontarotti, P. (ed.) *Evolutionary Biology: Self/Nonself Evolution, Species and Complex Traits Evolution, Methods and Concepts*. Cham, Springer.

Lemos, T. H., Da Cunha Tavares, V. & Moras, L. M. (2020). Character variation and taxonomy of short-tailed fruit bats from Carollia in Brazil. *Zoologica*, **37**, 1–7.

Nesi, N., Kadjo, B., Pourrut, X., Leroy, E., Shongo, C. P., Cruaud, C. & Hassanin, A. (2013). Molecular systematics and phylogeography of the tribe Myonycterini (Mammalia, Pteropodidae) inferred from mitochondrial and nuclear markers. *Molecular Phylogenetics and Evolution*, **66**, 126–137.

Novacek, M. J. (1985a). Evidence for echolocation in the oldest known bats. *Nature*, **315**, 140–141.

Novacek, M. J. (1985b). Comparative morphology of the bat auditory region. *Fortschritte der Zoologie*, **30**, 149–151.

Novacek, M. J. (1991). Aspects of the morphology of the cochlea in microchiropteran bats: an investigation of character transformation. *Bulletin of the American Museum of Natural History*, **206**, 84–100.

Orihuela, J. (2011). Skull variation of the vampire bat *Desmodus rotundus* (Chiroptera: Phyllostomidae): Taxonomic implications for the Cuban fossil vampire bat *Desmodus puntajudensis*. *Chiroptera Neotropical*, **17**, 863–876.

Prudent, X., Parra, G., Schwede, P., Roscito, J. G., & Hiller, M. (2016). Controlling for phylogenetic relatedness and evolutionary rates improves the discovery of associations between species' phenotypic and genomic differences. *Molecular Biology and Evolution*, **33**, 2135–2150.

Romagnoli , M. L. & Springer, M. S. (2000). Evolutionary relationships among Old World fruitbats (Megachiroptera: Pteropodidae) based on 12S rRNA, tRNA valine, and 16S rRNA gene sequences. *Journal of Mammalian Evolution*, **7**, 259–284.

Reyes-Amaya, N. & Jerez, A. (2013). Postnatal cranial ontogeny of the common vampire bat *Desmodus rotundus* (Chiroptera: Phyllostomidae). *Chiroptera Neotropical*, **19**, 1198–1211.

Sánchez, R. T., Montani, E. M., Tomasco, I. H. & Díaz, M. M. (2019). A new species of *Eptesicus* (Chiroptera, Vespertilionidae) from Argentina. *Journal of Mammalogy*, **100**, 118–129.

Sprague, J. M. (1943). The hyoid region of placental mammals with especial references to the bats. *American Journal of Anatomy*, **72**, 385–472.

Springer, M. (1995). Phylogeny, Molecules versus morphology, and rates of character evolution among fruitbats (Chiroptera: Megachiroptera). *Australian Journal of Zoology*, **43**, 557–582.

Springer, M. S., Teeling, E. C., Madsen, O., Stanhope, M. J., De Jong, W. W. (2001). Integrated fossil and molecular data reconstruct bat echolocation. *Proceedings of the National Academy of Sciences*, **98**, 6241–6246.

Teeling, E. C., Vernes, S. C., Dávalos, L. M., Ray, D. A., Gilbert, M. T. P., Myers, E. & Bat1k Consortium. (2018). Bat biology, genomes, and the Bat1K project: to generate chromosome-level genomes for all living bat species. *Annual Review of Animal Biosciences*, **6**, 23–46.

Tomkins, J. L. & Kotiaho, J. S. (2001). Fluctuating asymmetry. In: *Encyclopedia of Life Science*. London, MacMillian Reference Ltd.

Wible, J. R. & Bhatnagar, K. P. (1996). Chiropteran vomeronasal complex and the interfamilial relationships of bats. *Journal of Mammalian Evolution*, **3**, 285–314.

Wójcik, J. M., Polly, P. D., Wójcik, A. M. & Sikorski, M. D. (2007). Epigenetic variation of the common shrew, *Sorex araneus*, in different habitats. *Russian Journal of Theriology*, **6**, 43–49.

Zakharov, V. M., Pankakoski, E., Sheftel, B. I., Peltonen, A. & Hanski, I. (1991). Development stability and population dynamics in the common shrew, *Sorex araneus*. *American Naturalist* **138**, 797–810.